Strojniški vestnik - Journal of Mechanical Engineering 60(2014)9, 549-560
DOI:10.5545/sv-jme.2013.1600
Original Scientific Paper
Received for review: 2013-12-10
Received revised form: 2014-03-28
Accepted for publication: 2014-05-13

High-Cycle Fatigue Behavior of Austenitic Steel and Pure Copper under Uniaxial, Proportional and Non-Proportional Loading

Łukasz Pejkowski* – Dariusz Skibicki – Janusz Sempruch
University of Technology and Life Sciences in Bydgoszcz, Poland

Austenitic steel EN: X2CrNiMo17-12-2 (ASTM: 316L) and copper Cu-ETP (DIN: E-Cu58, EN: CW004A, ASTM: C11000) were subjected to tension-compression, torsion and complex loads, including non-proportional loads. The non-proportionality of the state of stress resulted from a phase shift of the value δ = 90° of load components with sine signals and variable ratio of shear to normal stress λ.

On the basis of the results, Wöhler's curves were prepared, presenting the dependency of fatigue life to equivalent stress levels. Their analysis shows that fatigue life is strictly connected with the value of coefficient λ. The existence of its critical value can also be observed, which results in the highest fatigue life reduction. The value is different for each material. Furthermore, fractographic tests were conducted showing the influence of the level and type of load on the fracture face.

Keywords: multi-axial fatigue, high cycle fatigue, non-proportional load, fractography, out-of-phase

0 INTRODUCTION

The negative impact of the non-proportionality of stress components on fatigue strength and fatigue life [1] and [2] was observed in relation to a significant number of materials. Its direct effect is the phenomenon of additional hardening [3] to [5]. Non-proportionality can result from periodic load signals with phase shift (Fig. 1a) [6] to [8], asynchronous periodic signals (Fig. 1b) and random signals (Fig. 1c) [9] to [11] among other factors

In cases of periodic out-of-phase signals of components of stress, the most damaging to the material, regardless of its type, is phase shift, expressed by the value of angle $\delta = 90°$. The degree of non-proportionality of stress condition also depends on the ratio of amplitudes of shear to normal stress $\lambda = \tau_a / \sigma_a$, which is usually omitted in works that analyse non-proportional loads.

The objective of the this study is to analyse the influence of the λ ratio on fatigue life and the fatigue fracture surface morphology and crack plane orientation (which often are the subject of interest [9], [12] and [13]) for copper Cu-ETP and austenitic steel X2CrNiMo17-12-2. The materials were selected for tests due to their potentially high sensitivity to non-proportionality of load [14].

1 TESTS CONDITIONS

All fatigue tests were conducted with application of a fully reversed sine signal ($R = -1$) of constant amplitude, with stress control, using an Instron 8874 biaxial testing system with a load range of ±25 kN for tension-compression and ±100 Nm for torsion (Fig. 2).

Specimens were made by the machining of material as delivered. Specimen dimensions are presented on Fig. 3. Chemical composition of the tested steel and copper type are presented in Tables 1 and 2.

The specimens were subject to tension-compression, torsion, proportional load ($\lambda = 0.5$) and non-proportional loads ($0.3 < \lambda < 0.8$, $\delta = 90°$).

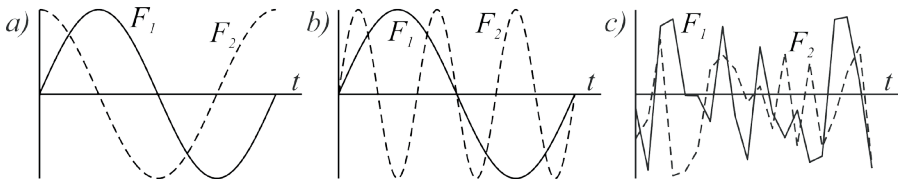

Fig. 1. *Examples of loads signals causing non-proportional condition of stress; a) out-of-phase load signals b) asynchronous load signals, and c) random load signals*

Table 1. *Chemical composition of X2CrNiMo17-12-2 steel (% weight)*

C	Si	Mn	Ni	P	S	Cr	Mo	N
<0.03	<1	<2	10 to 13	<0.045	<0.015	16.5 to 18.5	2 to 2.5	<0.11

*Corr. Author's Address: University of Technology and Life Sciences, Kordeckiego 20, Bydgoszcz, Poland, lukasz.pejkowski@utp.edu.pl

Table 2. *Chemical composition of Cu-ETP copper (% weight)*

Cu	Bi	O	Pb
>99.9	<0.0005	<0.04	<0.005

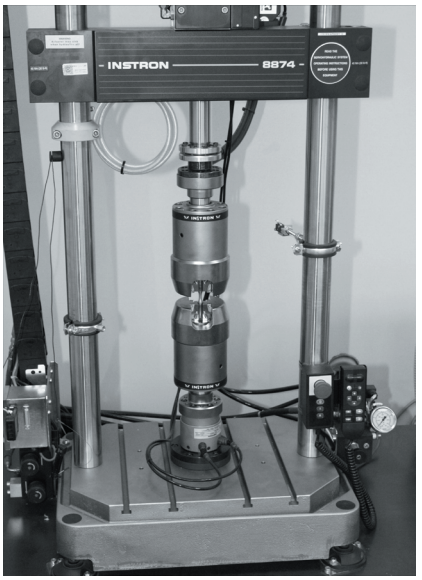

Fig. 2. *Instron 8874 biaxial testing system*

Values of amplitudes were selected in order to obtain the exact value of amplitude (denoted as in subscript) of root mean square of the second invariant of stress deviator, $\sqrt{J_{2,a}}$ [15], multiplied by fatigue limits ratio for a given load level. The value can be written as follows:

$$\sigma_{eq} = \frac{\tau_{-1}}{\sigma_{-1}}\sqrt{J_{2,a}} = const. \tag{1}$$

The above value is the equivalent stress according to von Mises criterion:

$$\sigma_{eq} = \sqrt{3}\sqrt{J_{2,a}}, \tag{2}$$

with consideration of fatigue limits ratio for torsion and tension-compression τ_{-1}/σ_{-1}, in place of the constant value $\sqrt{3}$. The von Mises criterion does not take into account the non-proportionality of load. The choice of such a criterion has been made deliberately, in order to show how the variable degree of non-proportionality, depending on the value of λ ratio, affects the fatigue life.

TC indicates the results for tension-compression, T is torsion, P5 proportional load of coefficient $\lambda = 0.5$ and non-proportional loads, expressed as *NP*, of values of coefficient $\lambda = 0.3$, 0.4, 0.5, 0.53, 0.6, 0.7, 0.8, respectively.

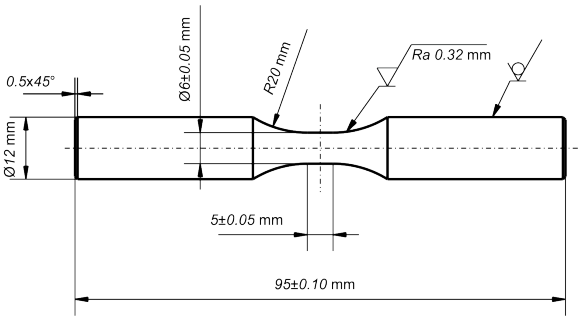

Fig. 3. *Geometry of tested specimens*

Fig. 4 shows state of stress on the surface of the specimen and distribution of normal stress σ_α, shear stress τ_α and von Mises equivalent stress $\sigma_{M\alpha}$ acting on specimen surface, depending on the direction expressed by α angle.

2 TEST RESULTS

2.1 Fatigue Life

A summary of the test results is presented in Tables 3 and 4.

Fig. 5 presents Wöhler's curves obtained for copper Cu-ETP. On the ordinate axis, the values of equivalent stress σ_{eq} (according to von Mises criterion) and on abscissa axis lives expressed with number of cycles *N* were identified. The curves were described with the Basquin equation:

$$\sigma_{eq} = AN^B, \tag{3}$$

coefficient *A* and exponent *B* of which were obtained via least square linear regression. The procedure of generating a line of best fit is well known in fatigue literature and its description can be found in [16] as well as in other sources. The resulting coefficients of determination *R*2 are denoted in Figs. 5 and 8. After transformation of the Basquin equation:

$$N = \left(\frac{\sigma_{eq}}{A}\right)^{\frac{1}{B}}, \tag{4}$$

it is possible to calculate the fatigue life as the material is supposed to reach for the specific value of equivalent stress. The values of equivalent stresses calculated for various loads were placed into a transformed Basquin's equation coefficients, which were determined for tension-compression; in this way the calculated fatigue lives N_{cal} were specified. Then they were compared with experimental fatigue lives

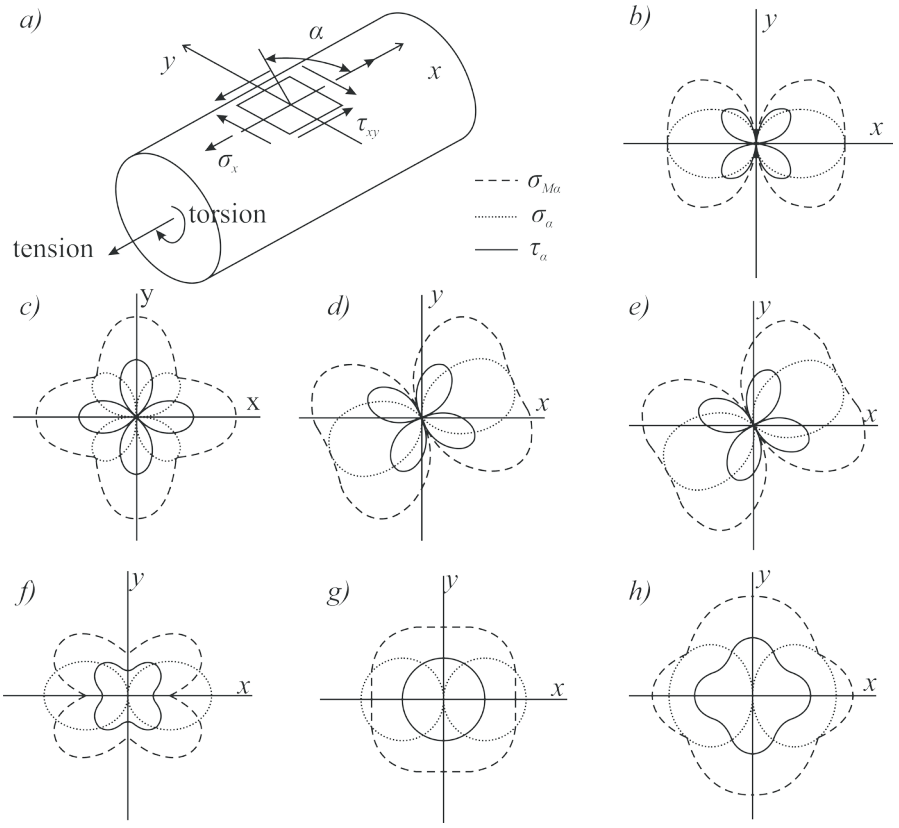

Fig. 4. *a) Out-of-phase tension-compression and torsion – state of stress illustrated b) distribution of Von Mises equivalent stress $\sigma_{M\alpha}$, normal stress σα and shear stress τα on a plane tangent to specimen surface in case of tension-compression, c) torsion, d) proportional tension-compression with torsion λ = 0.5, e) proportional tension-compression with torsion λ = 0.8, f) non-proportional tension-compression with torsion λ = 0.3, g) non-proportional tension-compression with torsion λ = 0.5, and h) non-proportional tension-compression with torsion λ = 0*

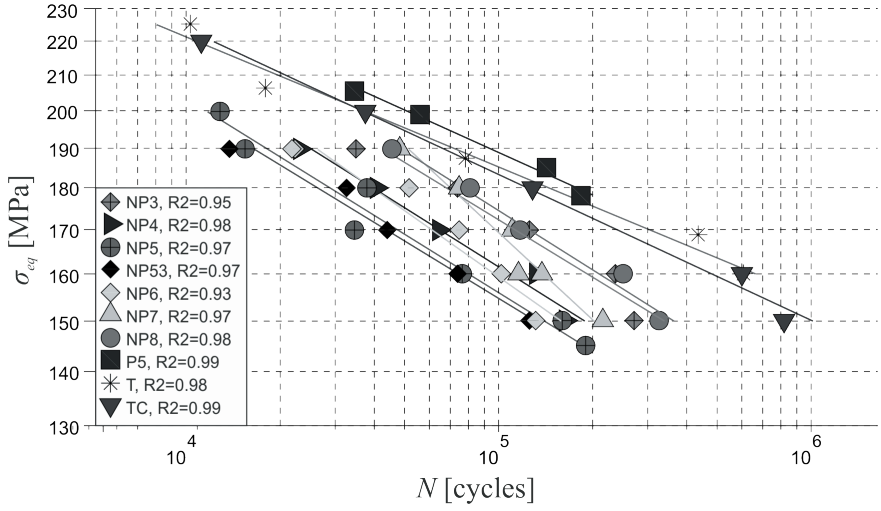

Fig. 5. *Wöhler's curves obtained for Cu-ETP copper for various load types*

N_{exp} achieved for tension-compression. Comparative results are presented in Fig. 6. Solid and dotted lines on the figure symbolize scatter bands, which indicate lives that are two and three times longer or shorter than experimental ones.

Fig. 7 presents a graph of dependency of fatigue life on λ at the level of equivalent stresses σ_{eq} = 160 MPa.

Analogously, the following were prepared: Wöhler's curves (Fig. 8), a fatigue life comparison

Table 3. *Test history for all fatigue specimens for Cu-ETP copper*

Specimen no.	Load type	σ_a [MPa]	τ_a [MPa]	δ [°]	N [no. of cycles]
2	TC	220	0	0	11,247
3	TC	200	0	0	37,432
4	TC	180	0	0	128,933
5	TC	150	0	0	816,270
73	TC	160	0	0	601,749
8	T	0	90	0	432,462
9	T	0	110	0	17,893
10	T	0	100	0	78,004
11	T	0	120	0	10,269
74	T	0	85.4	0	607,029
12	P5	130	65	0	184,190
13	P5	150	75	0	34,694
14	P5	135	67	0	142,212
15	P5	145	72	0	55,991
30	N3	170	51	90	125,877
22	N3	180	54	90	74,163
29	N3	190	57	90	35,145
55	N3	160	48	90	235,151
69	N3	150	45	90	272,506
46	N4	170	68	90	64,318
47	N4	180	72	90	40,812
48	N4	190	76	90	23,197
56	N4	160	64	90	130,741
70	N4	150	60	90	164,044
16	N5	145	72	90	189,644
17	N5	160	80	90	76,203
18	N5	180	90	90	37,971
19	N5	200	100	90	12,829
50	N5	170	85	90	34,726
51	N5	190	95	90	15,371
68	N5	150	75	90	159,779
52	N53	180	96	90	32,710
53	N53	170	90.7	90	44,034
54	N53	190	101.3	90	13,770
58	N53	160	85.3	90	73,917
67	N53	150	80	90	125,195
37	N6	151.1	90.7	90	74,900
35	N6	160	96	90	51,551
45	N6	169	101.4	90	22,322
49	N6	169	101.4	90	21,833
57	N6	142.2	85.3	90	101,644
71	N6	133.4	80	90	130,712
23	N7	137.1	96.0	90	74,395
31	N7	144.8	101.4	90	48,146
43	N7	129.6	90.7	90	110,808
59	N7	121.9	85.3	90	115,927
65	N7	121.9	85.3	90	137,314
72	N7	114.3	80	90	215,815
28	N8	113.4	90.7	90	117,308
20	N8	120	96.0	90	80,724
27	N8	126.7	101.4	90	45,681
60	N8	106.7	85.4	90	249,457
66	N8	100	80	90	326,218

graph (Fig. 9), and a graph of fatigue life dependency on λ (Fig. 10), for X2CrNiMo17-12-2 steel for tension-compression (*TC*), torsion (*T*), proportional load (*P*) of λ value 0.5 and 0.8 and non-proportional (*NP*) with $\lambda = 0.5$, 0.8 and 1.0.

In case of both tested materials, the fatigue lives of specimens subject to uniaxial load and proportional

Table 4. *Test history for all fatigue spec. for X2CrNiMo17-12-2 steel*

Specimen no.	Load type	σ_a [MPa]	τ_a [MPa]	δ [°]	N [no. of cycles]
1	TC	350	0	0	23,420
2	TC	350	0	0	14,937
3	TC	350	0	0	18,048
4	TC	330	0	0	75,013
5	TC	330	0	0	49,513
6	TC	330	0	0	68,038
7	TC	342	0	0	25,225
11	TC	325	0	0	139,108
8	TC	325	0	0	89,469
10	TC	311	0	0	199,142
9	TC	303	0	0	632510
15	TC	325	0	0	146,934
16	TC	311	0	0	147,769
21	TC	325	0	0	190,912
22	TC	325	0	0	112,227
23	TC	303	0	0	235,423
24	TC	311	0	0	174,567
72	TC	333.3	0	0	39,467
33	T	0	310	0	9,108
34	T	0	300	0	10,197
35	T	0	290	0	11,202
36	T	0	260	0	135,216
37	T	0	250	0	599,432
38	T	0	270	0	106,582
39	T	0	280	0	58,678
73	T	0	276	0	30,801
40	P5	270	135	0	167,175
41	P5	285	142.5	0	81,692
46	P5	299	149.8	0	14,444
71	P5	285	142.5	0	98,892
47	P8	247	204.6	0	35,318
48	P8	233	193.1	0	61,307
49	P8	219	181.4	0	215,220
42	N5	333	166.5	90	24,697
45	N5	320	160	90	45,993
54	N5	310	155	90	106,276
53	N5	300	150	90	127,454
61	N5	333	166.5	90	23,027
62	N5	320	160	90	62,307
63	N5	310	155	90	158,758
64	N5	300	150	90	368,041
70	N5	333	166.5	90	26,124
108	N6	310	186	90	35,742
112	N6	333	199,8	90	20,109
13	N6	320	192	90	27,697
114	N6	300	180	90	86,619
43	N8	333	275.1	90	12,810
44	N8	320	264.3	90	28,491
50	N8	310	256.1	90	28,341
51	N8	300	247.8	90	34,506
55	N8	333	275.1	90	10,264
56	N8	320	264.3	90	10,856
57	N8	310	256.1	90	29,734
58	N8	300	247.8	90	11,663
59	N8	320	264.3	90	23,124
60	N8	300	247.8	90	40,540
96	N10	260	260.0	90	30,219
105	N10	244	240	90	120,406
106	N10	251,8	251,8	90	46,128
107	N10	270,5	270,5	90	14,952
115	N12	203,1	243,7	90	67,318
116	N12	209,9	251,9	90	63,312
117	N12	216,6	259,9	90	40,951
118	N12	225,5	270,6	90	14,395

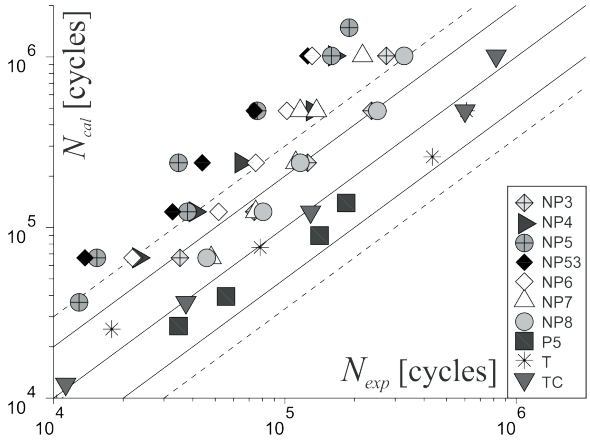

Fig. 6. *Comparison of experimental fatigue lives for tension-compression with calculated fatigue lives for Cu-ETP copper*

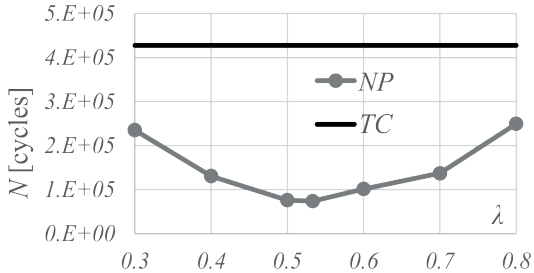

Fig. 7. *Dependency of fatigue life on λ for Cu- ETP, at the level of σ_{eq} = 160 MPa*

load, yielding the same value of equivalent stress σ_{eq}, are very close. At the same time, the fatigue life of specimens subject to non-proportional loads is lower. Fatigue life reduction significantly depends on λ. Its highest reduction in the case of copper can be observed for $\lambda = 0.53 \approx \tau_{-1}/\sigma_{-1}$, and for steel for $\lambda = 0.8 \approx \tau_{-1}/\sigma_{-1}$.

2.2 Macrofractography

Fig. 11 presents, on the background of Wöhler's curves, the images of fracture surfaces morphology and cracks of Cu-ETP specimens subject to tension-compression (*TC*). In all fracture surfaces, the tensile-mechanism, indicating mode and fracture load can be observed. Fracture is perpendicular to the load direction. There was Case A and B crack growth (Case A grew along the surface of a material; Case B grew into the depth of a material [3]). At higher load levels, there are ratchet marks visible, indicating the initiation of cracking with multiple origins and a relatively big fast fracture zone.

In Fig. 12, images of surface fracture morphology and Cu-ETP cracks from specimens being subjected to torsion are shown. Cracks were loaded in mode II, meaning that the shear mechanism operated. In all specimens, the direction of macro-crack is compliant with the direction of maximum shear stress.

Fig. 13 shows images of surface fracture morphology and Cu-ETP cracks from specimens being subjected to a proportional load of coefficient $\lambda = 0.5$. The fracture face of the most loaded specimen resembles the fracture face of a specimen subject to tension-compression of low stress value. There are no ratchet marks and many origins, and the fracture

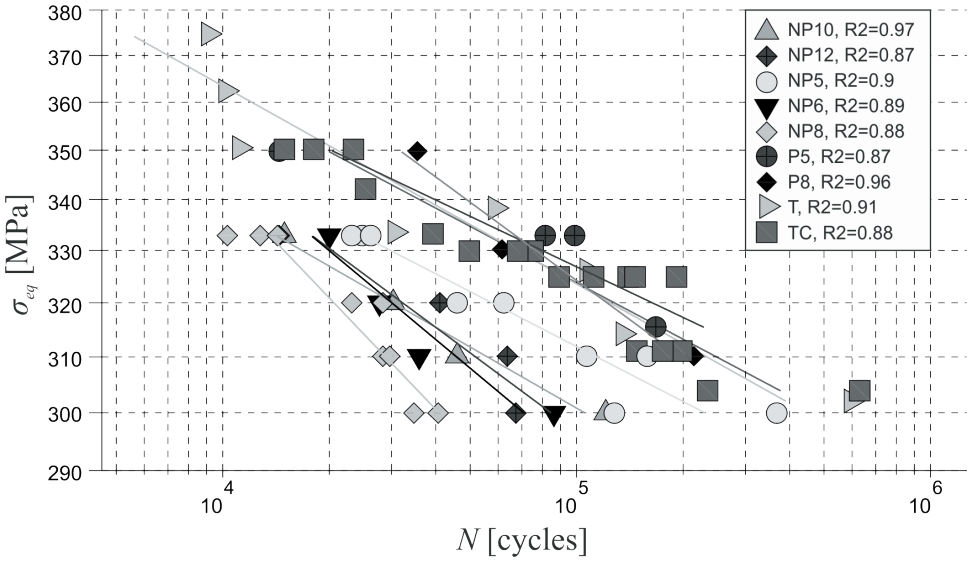

Fig. 8. *Wöhler's curves obtained for X2CrNiMo17-12-2 steel for various load types*

zone is relatively small. One can observe more crack growth in Case A than in a case of pure shear. The higher the load level, the greater the number of origins and ratchet marks, being inclined and tapered, indicating the participation of torsion.

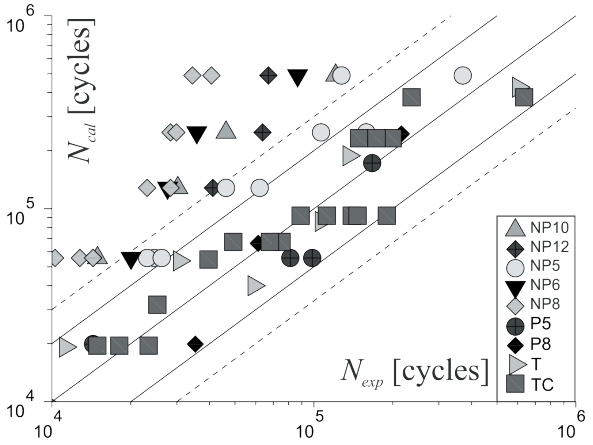

Fig. 9. *Comparison of experimental fatigue lives for tension-compression with calculated fatigue lives for X2CrNiMo17-12-2 steel*

Images of surface fracture morphology and cracks in Cu-ETP specimens for non-proportional loads of three various values of coefficient λ are presented in Fig. 14. In the case of $\lambda = 0.3$, surface fractures of the most highly loaded specimen, is as for the specimen subject to tension-compression. There are no ratchet marks, and in the vicinity of the fracture zone there are several progression marks visible. The macro-crack plane is perpendicular to the specimen axis. On the fracture surface of specimens subject to lower loads, there are many river marks visible. Their endings indicate the fracture propagated in many directions. The macro-crack plane is located at an angle of 45° in relation to the specimen axis. For $\lambda = 0.5$, the fracture surface of the specimen subject to the highest loads is characterised by and extremely large fracture zone meaning that the material was under significant stress. The surface of the fatigue zone is irregular and the crack propagated from many origins and on various planes. In the case of a specimen subject to load of the lowest value, the fracture zone is smaller and fatigue zone as well as the macro-crack also indicate that the crack propagated on many planes.

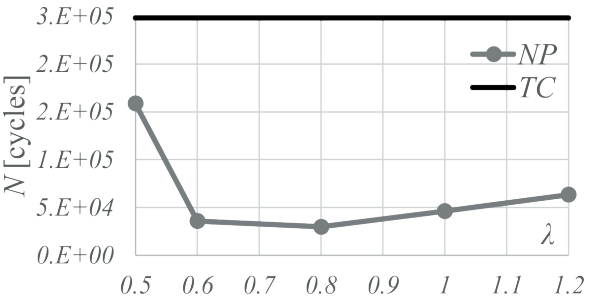

Fig. 10. *Dependency of fatigue life on λ for X2CrNiMo17-12-2 steel, at the level of σ_{eq} = 310 MPa*

The predominance of Case A crack growth is visible. The macro-crack of the specimen subject to a non-proportional load of coefficient $\lambda = 0.7$, of the highest value is perpendicular to the specimen axis.

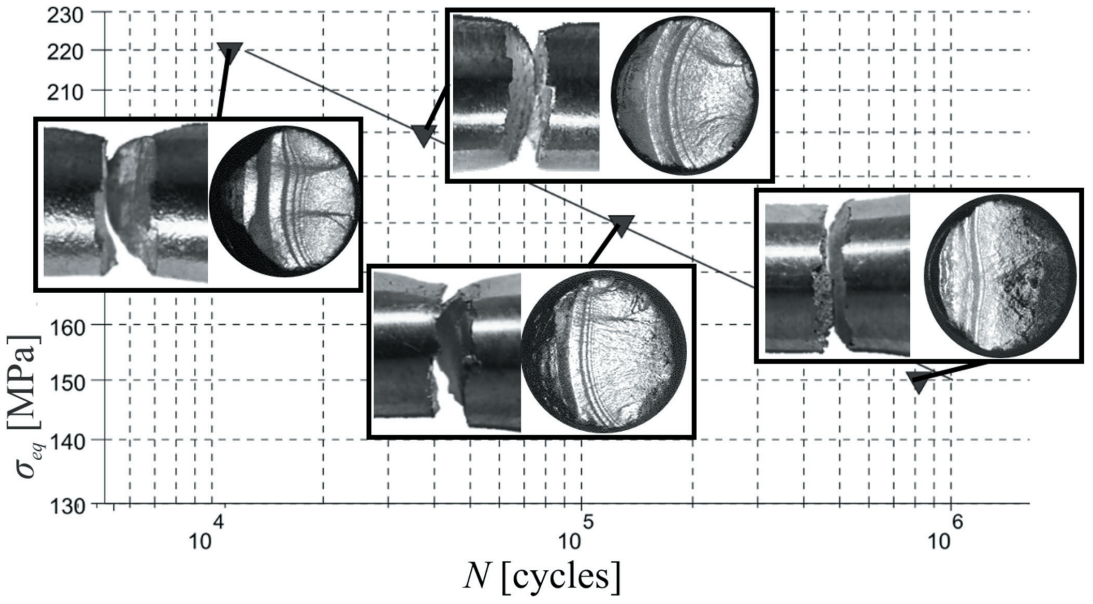

Fig. 11. *Fractography of Cu-ETP for tension-compression*

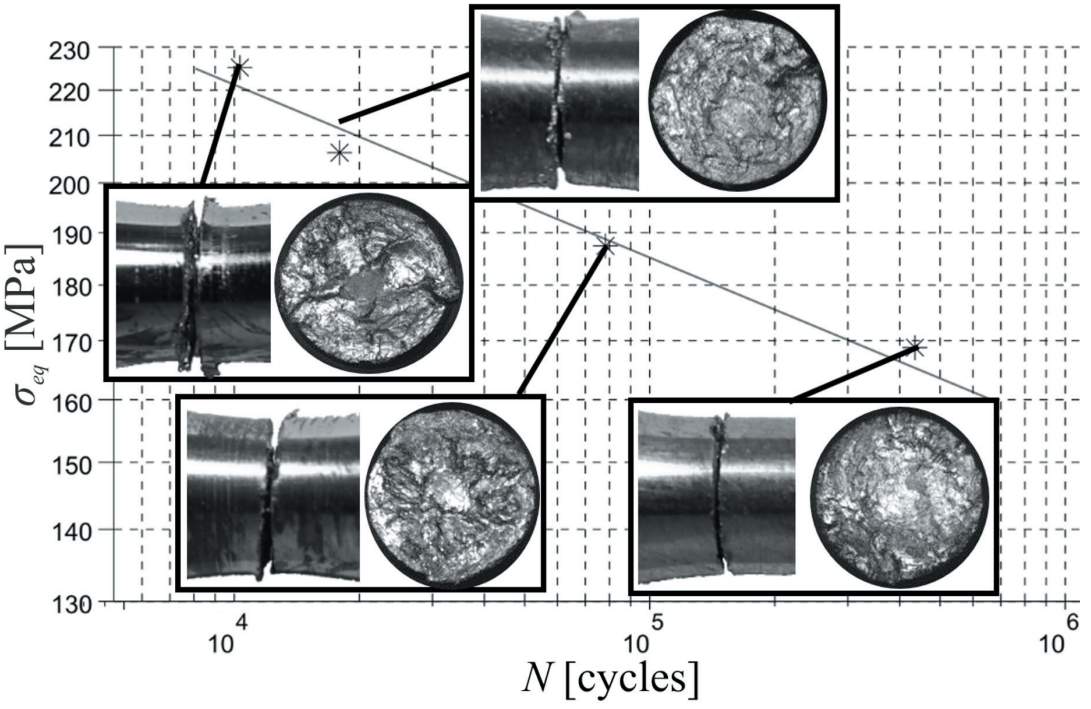

Fig. 12. *Fractography of Cu-ETP for torsion*

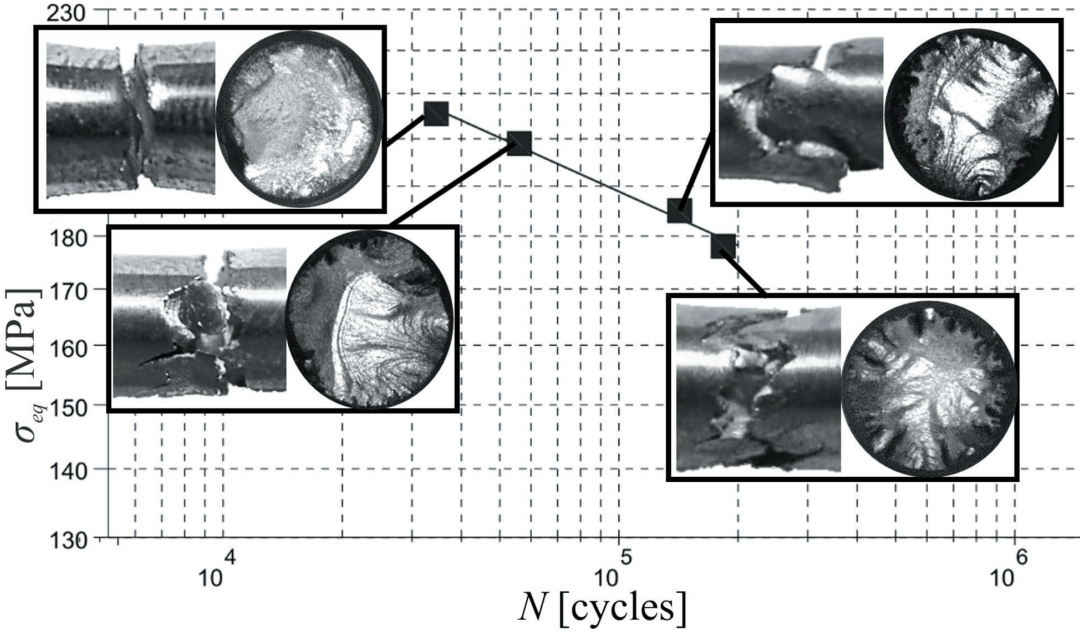

Fig. 13. *Fractography of Cu-ETP for proportional load (λ = 0.5)*

The predominance of Case A crack growth is even higher and the fracture surface bears friction marks. The macro-crack and fracture surface of the specimen subject to loads of lower value indicate cracks in many origins and crack development on a greater number of planes.

To summarize, the characteristic feature of fracture surfaces of copper specimens subject to non-proportional load is the crack growth on many planes.

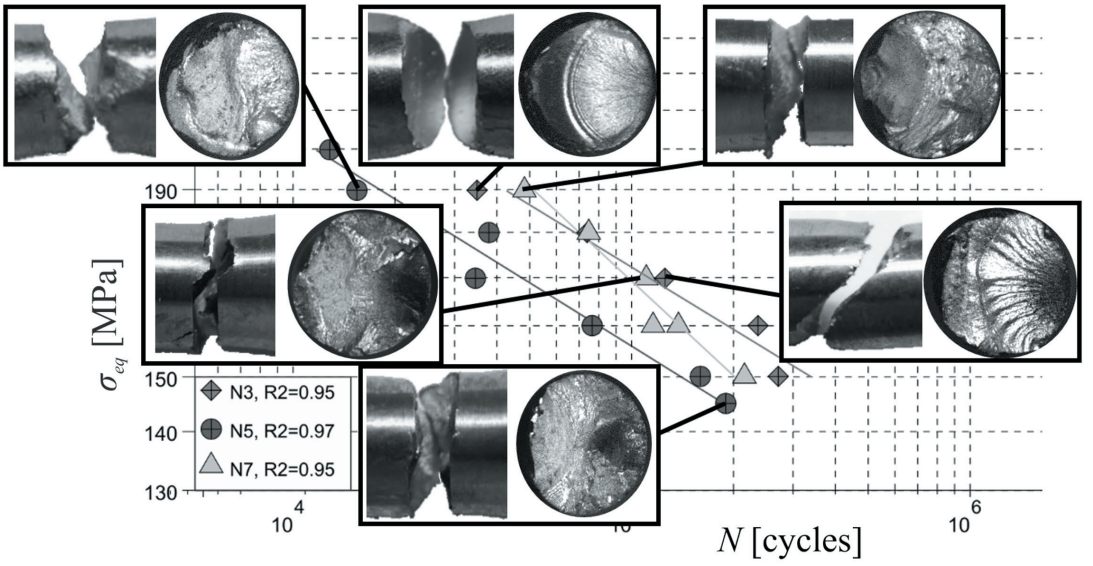

Fig. 14. *Fractography of Cu-ETP for non-proportional loads (λ = 0.3, 0.5 and 0.7)*

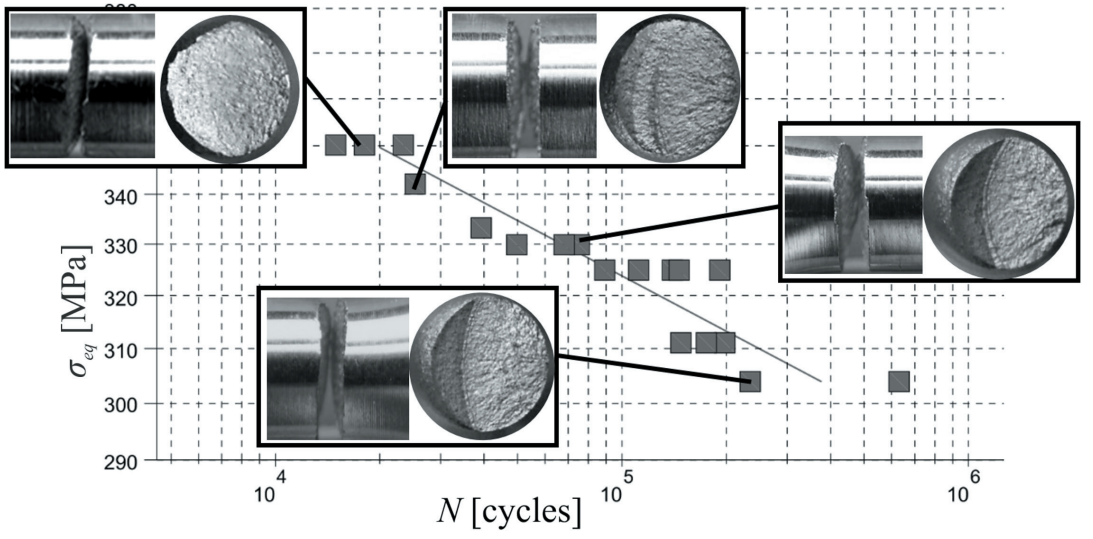

Fig. 15. *Fractography of X2CrNiMo17-12-2 for tension-compression*

Fig. 15 presents fracture surfaces morphology and cracks of specimens made of steel X2CrNiMo17-12-2, subject to tension-compression. The tensile mechanism causing the Case A and B crack growth can be observed. The fracture is perpendicular to the load direction. In the fatigue zone, there are no progression marks or ratchet marks. The crack initiation was of a single origin. The fracture zone decreases along with the load reduction.

Fig. 16 shows fracture surfaces morphology and specimen cracking of X2CrNiMo17-12-2, which were subject to fully reversed torsion. In cases with a high load level, the crack direction is compliant with the direction of maximum shear stress. There is a Case A crack growth. The fracture surface is featureless due to friction. The reduction of load level caused the change of macro-crack direction by 45°. For medium load levels, one can observe that the crack propagated on two planes, whilst for the lower load level only on a single plane.

Fracture surfaces and cracks of X2CrNiMo17-12-2 specimens subject to proportional loads of coefficient values $\lambda = 0.5$ and 0.8 are presented in Fig. 17. In the case of $\lambda = 0.5$, cracks propagated at

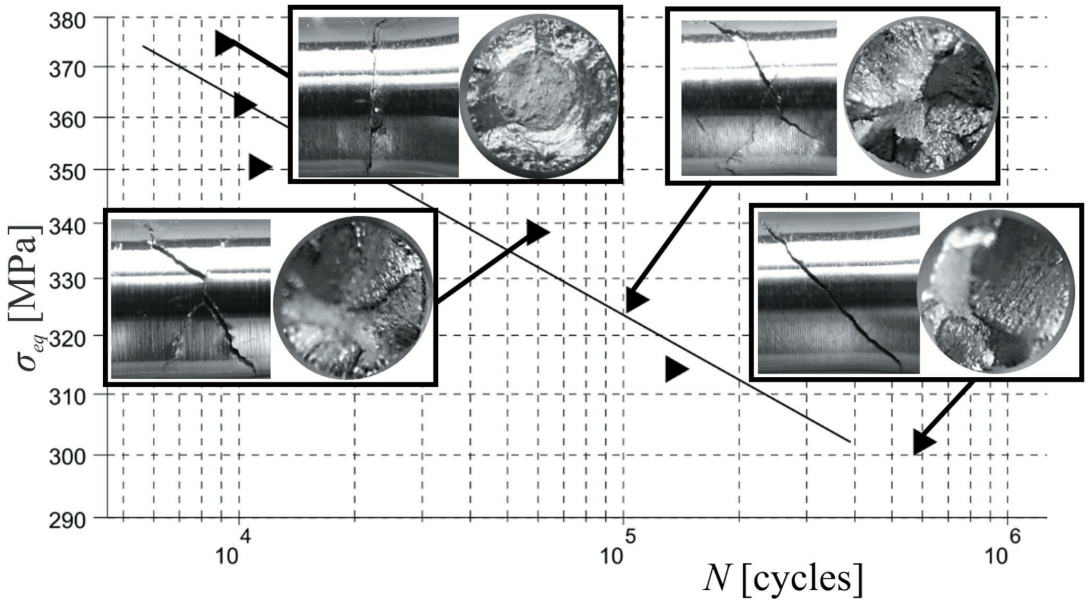

Fig. 16. *Fractography of X2CrNiMo17-12-2 for torsion*

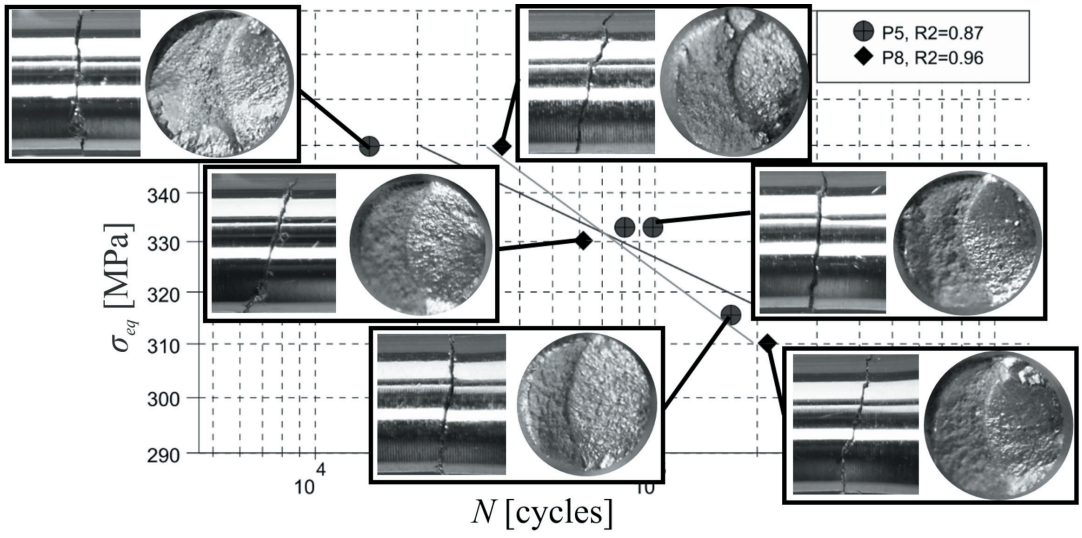

Fig. 17. *Fractography of X2CrNiMo17-12-2 for proportional load (λ = 0.5, 0.8)*

the angle of 7°, and for $\lambda = 0.8$ at the angle of 15°. The difference is 8°, and it is identical with the value of change of angle of principal axes between these load cases. Fracture surfaces are similar to fracture surface for tension-compression with the difference that the crack propagated more inward with regards to the material (Case B), rather than along the crack length.

Fig. 18 shows fracture faces morphology and cracks of X2CrNiMo17-12-2 steel specimens subject to non-proportional loads of coefficient values $\lambda = 0.5$ and 0.8. In cases of $\lambda = 0.5$, the crack propagated along perpendicular direction to the specimen axis and more inwards with regard to the material (Case B) than for $\lambda = 0.5$ (more torsion), where it propagated more along the direction of the crack length (Case A) and at an angle of 30°.

Load non-proportionality resulted in the crack surface and its edge being highly irregular, indicating that the crack propagated on various planes. Similar to the case of Cu-ETP, the characteristic feature of fracture surfaces of specimens subject to non-proportional load is the crack propagation on many planes.

Table 5. *Summary of fracture features for Cu-ETP copper*

		Tension	Torsion	Proportional	Non-proportional		
		$\lambda = 0$	$\lambda = \infty$	$\lambda = 0.5$	$\lambda = 0.3$	$\lambda = 0.5$	$\lambda = 0.7$
High stresses	Macro fracture plane direction	$\perp\sigma_{1\max}$	$\|\|\tau_{\alpha\max}$	$\perp\sigma_{1\max}$	$\perp\sigma_{1\max}$	$\perp\sigma_{1\max}$	$\perp\sigma_{1\max}$
	Crack growth case	A ≈ B	A	A ≈ B	A ≈ B	A ≈ B	A >> B
	Number of origins	multiple	multiple	multiple	single	single	single
	Ratchets marks presence	yes	no	tapered	no	no	yes
	Progression marks / river marks presence	yes / no	no / no	no / no	yes / no	no / no	no / no
Low stresses	Macro fracture plane direction	$\perp\sigma_{1\max}$	$\|\|\tau_{\alpha\max}$	$\perp\sigma_{1\max}$	$\|\|\tau_{\alpha\max}$	$\perp\sigma_{1\max}$	$\perp\sigma_{1\max}$
	Crack growth case	A ≈ B	A	difficult to identify	A ≈ B	A > B	A >> B
	Number of origins	single	multiple	multiple	single	single	single
	Ratchets marks presence	no	no	tapered	tapered	no	no
	Progression marks / river marks presence	yes / no	no / no	no / no	no / yes	no / no	no / no

Table 6. Summary of fracture features for X2CrNiMo17-12-2 steel

		Tension	Torsion	Proportional		Non-proportional	
		$\lambda = 0$	$\lambda = \infty$	$\lambda = 0.5$	$\lambda = 0.8$	$\lambda = 0.5$	$\lambda = 0.8$
High stresses	Macro-fracture plane direction	$\perp\sigma_{1\max}$	$\|\|\tau_{\alpha\max}$	difficult to identify	difficult to identify	$\perp\sigma_{M\max}$	$\perp\sigma_{M\max}$
	Crack growth case	A ≈ B	A	B ≈ A	A ≈ B	A ≈ B	A >> B
	Number of origins	single	multiple	single	multiple	single	single
	Ratchets marks presence	no	no	no	no	no	no
	Progression marks / river marks presence	no / no	no / no	no / no	no / no	no / no	no / no
Low stresses	Macro-fracture plane direction	$\perp\sigma_{1\max}$	$\perp\sigma_{1/2\max}$	difficult to identify	difficult to identify	$\perp\sigma_{M\max}$	$\perp\sigma_{M\max}$
	Crack growth case	A ≈ B	A	B ≈ A	A ≈ B	A ≈ B	A >> B
	Number of origins	single	multiple	single	single	single	single
	Ratchets marks presence	no	no	no	no	no	no
	Progression marks / river marks presence	no / no	no / no	no / no	no / no	no / no	no / no

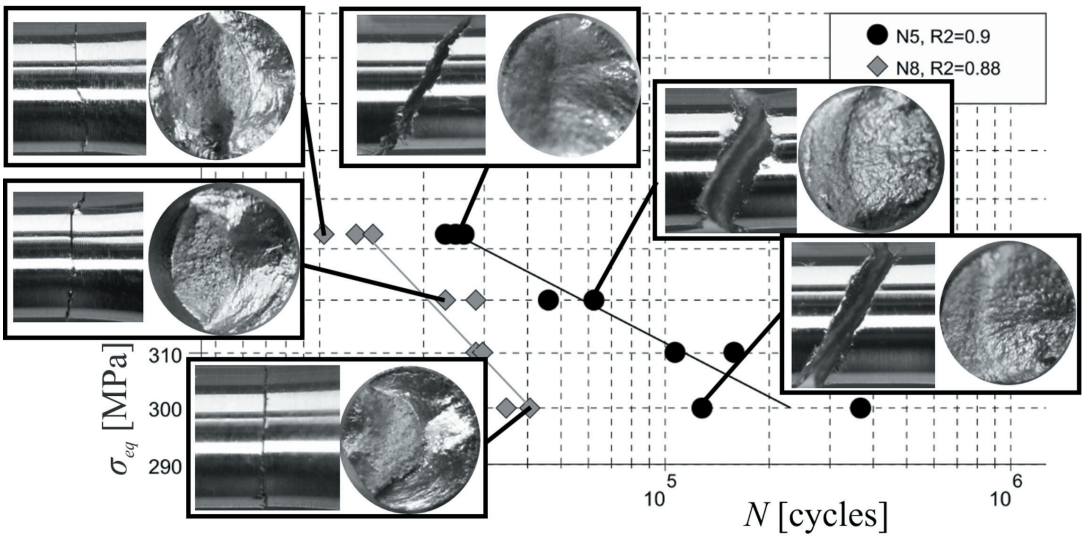

Fig. 18. *Fractography of X2CrNiMo17-12-2 for non-proportional loads (λ = 0.5, 0.8)*

The summaries of fracture features are presented in Tables 5 and 6.

Fracture surfaces of specimens subjected to non-proportional loads are different than for specimens subjected to proportional loads. Generally, in cases of non-proportional loads, cracks grow on many planes, thus the fracture surfaces are irregular.

Similarly to fatigue lives, the features of fracture surfaces strongly depend on the λ ratio. For high values of λ, more Case A than B crack growth mode can be observed, while in the case of proportional loads there was a similar amount of Case A and B crack growth mode. The influence of the most damaging value of λ ratio is also visible. Fracture surfaces are most irregular for the most non-proportional load, and cracks nucleated from many origins and propagated on many planes. The fracture zones are large, which indicates a high stress level.

3 SUMMARY AND CONCLUSIONS

A detailed study of the impact of shear to normal stress amplitudes, $\lambda = \tau_a/\sigma_a$, on the fatigue life and fracture surface morphology of materials sensitive to non-proportional loadings has been conducted.

Both tested materials showed high sensitivity to non-proportionality of load. In the case of Cu-ETP copper application of fatigue criterion in a manner stressing the impact of non-proportional loads, it resulted in over-estimation of fatigue strength by about 22% and fatigue life by about 450% in extreme cases. ForX2CrNiMo17-12-2 steel, it was ca. 10% and ca. 650%, respectively.

For both materials the value of shear to normal stress ratio λ had significant impact on fatigue life. Values of coefficient λ close to relation τ_{-1}/σ_{-1} turned out to be the most damaging both for copper and for austenitic steel.

A similar dependence on the value of the λ ratio was observed in case of fracture surfaces. It had an impact on their morphology and the orientation of the macro-fracture plane.

It is worth emphasizing that for both materials the critical value of λ was different. This allows for the creation of the hypothesis that for materials subject to out-of-phase loads the most damaging are loads with components shifted in phase by 90° and of shear-to-normal stress ratio equal to τ_{-1}/σ_{-1}.

Therefore, it seems that for estimation of fatigue strength and fatigue life in the conditions of non-proportional loads, the relation of fatigue limits τ_{-1}/σ_{-1} is of very high importance.

The microscopic models of non-proportional fatigue failure mechanisms are highly general, regardless of the material (steel [17], aluminium alloy [18], non-ferrous metals, [19] to [21], general (hypothetic) [22]). At this stage of research, it is difficult to directly show their relationship with macroscopic phenomena presented in the article.

4 ACKNOWLEDGEMENT

The project has been financed by the Polish National Science Centre. Project number: N N501 120940.

5 REFERENCES

[1] McDiarmid, D.L. (1986). Fatigue under out-of-phase bending and torsion. *Fatigue & Fracture of Engineering Materials & Structures*, vol. 9, no. 6, p. 457-475, DOI:10.1111/j.1460-2695.1987.tb00471.x.

[2] Ellyin, F., Golos, K., Xia, Z. (1991). In-phase and out-of-phase multiaxial fatigue. *Journal of Engineering Materials and Technology-Transactions of the ASME*, vol. 113, no. 1, p. 112-118, DOI:10.1115/1.2903365.

[3] Socie, D.F., Marquis, G.B. (1999). *Multiaxial Fatigue*. SAE International, Washington D.C.

[4] Fatemi, A., Shamsaei, N. (2011). Multiaxial fatigue: An overview and some approximation models for life estimation. *International Journal of Fatigue*, vol. 33, no. 8, p. 948-958, DOI:10.1016/j.ijfatigue.2011.01.003.

[5] Noban, M., Jahed, H., Ibrahim, E., Ince, A. (2012). Load path sensitivity and fatigue life estimation of 30CrNiMo8HH. *International Journal of Fatigue*, vol. 37, no. p. 123-133, DOI:10.1016/j.ijfatigue.2011.10.009.

[6] Zenner, H., Simburger, A., Liu, J. (2000). On the fatigue limit of ductile metals under complex multiaxial loading. *International Journal of Fatigue*, vol. 22, no. 2, p. 137-145, DOI:10.1016/S0142-1123(99)00107-3.

[7] Verreman, Y., Guo, H. (2007). High-cycle fatigue mechanisms in 1045 steel under non-proportional axial-torsional loading. *Fracture of Engineering Materials & Structures*, vol. 30, no. 10, p. 932-946, DOI:10.1111/j.1460-2695.2007.01164.x.

[8] Papadopoulos, I.V. (2001). Long life fatigue under multiaxial loading. *International Journal of Fatigue*, vol. 23, no. 10, p. 839-849, DOI:10.1016/S0142-1123(01)00059-7.

[9] Karolczuk, A. (2006). Plastic strains and the macroscopic critical plane orientations under combined bending and torsion with constant and variable amplitudes. *Engineering Fracture Mechanics*, vol. 73, no. 12, p. 1629-1652, DOI:10.1016/j.engfracmech.2006.02.005.

[10] Marciniak, Z., Rozumek, D., Macha, E. (2008). Fatigue lives of 18G2A and 10HNAP steels under variable amplitude and random non-proportional bending with torsion loading. *International Journal*

of Fatigue, vol. 30, no. 5, p. 800-813, DOI:10.1016/j.ijfatigue.2007.07.001.

[11] Banvillet, A., Łagoda, T., Macha, E., Niesłony, A, Palin-Luc, T., Vittori, J.-F. (2004). Fatigue life under non-gaussian random loading from various models. *International Journal of Fatigue*, vol. 26, no. 4, p. 349-363, DOI:10.1016/j.ijfatigue.2003.08.017.

[12] Roy, M., Nadot, Y., Maijer, D.M., Benoit, G. (2012). Multiaxial fatigue behaviour of A356-T6. *Fatigue & Fracture of Engineering Materials & Structures*, vol. 35, no. 12, p. 1148-1159, DOI:10.1111/j.1460-2695.2012.01702.x.

[13] Zhang, J., Shi, X., Bao, R., Fei, B. (2011). Tension–torsion high-cycle fatigue failure analysis of 2A12-T4 aluminum alloy with different stress ratios. *International Journal of Fatigue*, vol. 33, no. 8, p. 1066-1074, DOI:10.1016/j.ijfatigue.2010.12.007.

[14] Borodii, M.V., Shukaev, S.M. (2007). Additional cyclic strain hardening and its relation to material structure, mechanical characteristics, and lifetime. *International Journal of Fatigue*, vol. 29, no. 6, p. 1184-1191, DOI:10.1016/j.ijfatigue.2006.06.014.

[15] Papadopoulos, I.V., Davoli, P., Gorla, C., Filippini, M., Bernasconi, A. (1997). A comparative study of multiaxial high-cycle fatigue criteria for metals. *International Journal of Fatigue*, vol. 19, no. 3, p. 219-235, DOI:10.1016/S0142-1123(96)00064-3.

[16] Lee, Y.L., Pan, J., Hathaway, R., Barkey, M. (2004). *Fatigue Testing and Analysis*. Butterworth-Heinemann, Oxford.

[17] Kida, S., Itoh, T., Sakane, M., Ohnami, M., Socie, D. F. (1997). Dislocation Structure and Non-Proportional Hardening of Type 304 Stainless Steel. *Fatigue & Fracture of Engineering Materials & Structures*, vol. 20, no. 10, p. 1375-1386, DOI:10.1111/j.1460-2695.1997.tb01496.x.

[18] Zhang, J., Shi, X., Fei, B. (2012). High cycle fatigue and fracture mode analysis of 2A12–T4 aluminum alloy under out-of-phase axial–torsion constant amplitude loading. *International Journal of Fatigue*, vol. 38, p. 144-154, DOI:10.1016/j.ijfatigue.2011.12.017.

[19] Bentachfine, S., Pluvinage, G. (1996). Biaxial low cycle fatigue under non-proportional loading of a magnesium-lithium alloy. *Engineering Fracture Mechanics*, vol. 54, no. 4, p. 513-522, DOI:10.1016/0013-7944(95)00223-5.

[20] Zhang, J., Jiang, Y. (2005). An experimental investigation on cyclic plastic deformation and substructures of polycrystalline copper. *International Journal of Plasticity*, vol. 21, no. 11, p. 2191-2211, DOI:10.1016/j.ijplas.2005.02.004.

[21] Ding, X., He, G., Chen, C. (2010). Study on the dislocation sub-structures of Al–Mg–Si alloys fatigued under non-proportional loadings. *Journal of Materials Science*, vol. 45, no. 15, p. 4046-4053, DOI:10.1007/s10853-010-4487-3.

[22] Colak, U.O. (2004). A viscoplasticity theory applied to proportional and non-proportional cyclic loading at small strains. *International Journal of Plasticity*, vol. 20, no. 8-9, p. 1387-1401, DOI:10.1016/j.ijplas.2003.07.002.